Raman Spectroscopy and Low-Temperature Transport Measurements of Individual Single-Walled Carbon Nanotubes with Varying Thickness

ARTICLE *in* THE JOURNAL OF PHYSICAL CHEMISTRY C · AUGUST 2009

Impact Factor: 4.77 · DOI: 10.1021/jp9034985

5 AUTHORS, INCLUDING:

Olli Herranen
University of Jyväskylä
12 PUBLICATIONS **35** CITATIONS
SEE PROFILE

Andreas Johansson
University of Jyväskylä
26 PUBLICATIONS **524** CITATIONS
SEE PROFILE

Raman Spectroscopy and Low-Temperature Transport Measurements of Individual Single-Walled Carbon Nanotubes with Varying Thickness

Jyri Rintala,[†] Olli Herranen,[‡] Andreas Johansson,[‡] Markus Ahlskog,[‡] and Mika Pettersson*,[†]

Nanoscience Center, Department of Chemistry, University of Jyväskylä, P.O. Box 35, FI-40014, Finland, and Nanoscience Center, Department of Physics, University of Jyväskylä, P.O. Box 35, FI-40014, Finland

Received: April 16, 2009; Revised Manuscript Received: July 3, 2009

We have investigated two metallic and one semiconducting individual single-walled carbon nanotubes (SWNT) and one bundle of two semiconducting nanotubes with a diameter range 1.1−2.9 nm with Raman spectroscopy and low-temperature electric transport measurements. With these two methods, we obtain mutually independent measurements on the basic properties of a specific nanotube. In particular, we obtain data on metallic and semiconducting properties. Evidence of a small band gap for one metallic tube was obtained. For the semiconducting SWNTs with diameters of 2.7−2.9 nm, a special resonance condition was observed which causes an anomalous intensity ratio for the two components of the G-band. This effect has been observed previously for a few tubes with a diameter of 1.6 nm (Jorio, A; et al. *Phys. Rev. B* **2002**, *65*, 155412), and our current findings are in agreement with the previously given explanation of the effect and suggest that the effect is common among thick SWNTs. We also obtain evidence that the currently used relations between the frequency of the radial breathing mode and the tube diameter tend to underestimate the diameter for thick tubes.

Introduction

Carbon nanotubes (CNTs), especially single-walled (SWNTs), are extraordinary nanoscale realizations of one-dimensional conductors.[1] The diameters of SWNTs are usually in the range of 1−2 nm, while the length may exceed 100 μm. Even at the more typical length of a few micrometers, the aspect ratio is astonishingly high. Depending on the symmetry, the carbon nanotubes exist in both metallic and semiconducting forms. Due to this variability and the promise of technological applications, the recent decade has witnessed much research work being done on the electronic and optical properties of SWNTs.

Raman spectroscopy has been widely used for characterizing SWNTs because it is one of the most sensitive and informative spectroscopic methods to analyze this kind of nanostructure.[2,3] Spectroscopic measurements were earlier limited to bulk samples, but since a few years back, single-tube studies have been undertaken.[4−7] This has made it possible to study the dependence on diameter and chirality of each feature of Raman spectra of SWNTs. In order to analyze the resonance Raman spectra, it is useful to plot the resonance transition energies as a function of tube diameter for all SWNTs.[5] This so-called Kataura plot shows that the transition energies E_{ii} of each band are approximately inversely proportional to tube diameter d_t.[8−11] This allows to determine the diameter d_t and nanotube chirality, θ, of a specific (n,m) SWNT after the measurement of the frequency of the RBM and the resonant energy E_{ii}.[12] Once the (n,m) indices are identified, the dependence of the frequency and intensity of each of the features in the Raman spectra on diameter and chiral angle can be found, including the RBM, G-band, D-band, G′-band, and various overtone and combination modes within the first-order and higher-order frequency regions.[5] Nowadays, Raman spectroscopy is frequently used to make an assignment of chiral indices and to obtain detailed information at a single nanotube level.

Electronic transport in SWNTs is a rich subfield due to the existence of both metallic and semiconducting types and the long mean free path attainable in high quality tubes, as has been demonstrated in ballistically conducting single-SWNT devices.[13] Due to the inverse relation between the band gap and diameter in semiconducting SWNTs, in smaller SWNTs the gap is thus large enough that it totally dominates the transport at room temperature. A combination of Raman spectroscopy and electronic transport measurements is highly valuable by giving data on the electronic properties in mutually independent ways. Previous work on combined Raman and conductance measurements on SWNTs include both assemblies of tubes (ropes, parallel single tubes, or macroscopic amounts)[14−16] and experiments on individual tubes.[17−23] Among the latter, highly significant results on the gate voltage dependence of the G-mode has been observed. As one shifts the electron density in a SWNT with a gate voltage, the G-mode sensitively follows these changes via the electron−phonon coupling.[18,22]

In this study we separately measure low-temperature conductance and perform Raman spectroscopy on the same individual SWNTs which are electrically connected in a three-terminal configuration, that is, with source, drain, and gate electrodes. Raman spectroscopy is used to identify the tube type and to make an assignment of the chiral indices of the tubes. The transport measurements allow distinguishing the metallic or semiconducting character of the tubes and the low-temperature measurements, in particular, allow obtaining information on the small band gap of the metallic tubes. The diameters of the tubes vary between 1.1 and 2.9 nm and RBM mode is observed even for the thickest tubes which is usually difficult. In addition, for the thick tubes an anomalous intensity ratio of the G^+ and G^- bands is observed confirming the observations and predictions of Jorio et al.[24]

* To whom correspondence should be addressed. E-mail: mika.j.pettersson@jyu.fi.
[†] Department of Chemistry.
[‡] Department of Physics.

10.1021/jp9034985 CCC: $40.75
Published on Web 07/30/2009

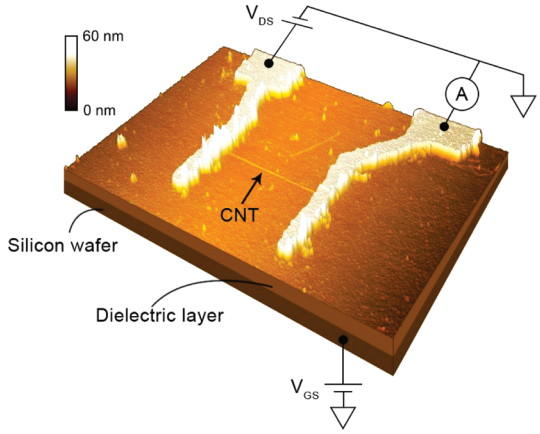

Figure 1. AFM image of sample S1. The measurement setup is schematically drawn in the image, with the underlying substrate acting as a backgate. The diameter of the CNT is ~2.5 nm, and the spacing between the drain and source electrodes is 880 nm. Another CNT above the contacted one can be observed separately in Raman measurements as discussed in the text.

Experimental Methods

Fabrication of the Sample. The samples were fabricated with standard e-beam lithography on top of a highly p-doped silicon substrate, covered by a 300 nm thick insulating layer of thermally grown SiO_2. The sample processing contained two different patterning steps. In the first step, a 6 × 6 alignment marker matrix (with a marker spacing of 7 μm) surrounded by 28 electrodes was patterned onto the substrate. Electron beam evaporation of 5 nm Ti layer was used to improve the adhesion before evaporating a 15 nm thick Pd layer followed by lift-off. Subsequently, the tubes were deposited on top of the surface and located with an atomic force microscope (AFM), using tapping mode imaging (see Figure 1). Finally a second exposure was done to contact the selected nanotubes to the surrounding electrodes. For this step, in which the contacts to the CNTs were made, only a single 20 nm thick Pd layer was used. We used commercial SWNTs (Nanocyl, 1100-series) which have an average diameter of 2 nm. The SWNT powder was dissolved in 1,2-dichloroethane and sonicated slightly before spin deposition onto the substrate.

Raman Measurements. The Raman measurements were performed with a home-built Raman spectrometer in a backscattering geometry using two different excitation wavelengths: 532 (Alphalas, Monolas-532-100-SM) and 632.8 nm (Melles Griot, 25-LHP-991-230). The coarse sample positioning was done with manual XYZ-stage (Newport, ULTRAling 462-XYZ-M) and the fine-tuning with XYZ-piezoscanner (Attocube, ANPxyz101) with a smallest step of 50 nm in each direction. The spectral resolution for this setup with 600 g/mm grating is 3−4 cm^{-1} measured from the fwhm (full width at half maximum) of the Rayleigh scattering peak. The excitation light was focused to a sample with a microscope objective (Olympus 100×, 0.70 N.A.) and the backscattered light was collected with the same objective. A beam splitter, an extra lens and a 10× microscope ocular was added to the setup to construct an optical microscope with 1000× magnification. This was needed to be able to visually inspect and pinpoint the excitation spot to desired area. The alignment mark matrix patterned earlier to the substrate was used to locate the tubes that were earlier spotted by AFM and contacted to the electrodes. The Rayleigh scattering was attenuated with an edge filter (Semrock) allowing recording of Raman spectrum down to 70 cm^{-1} when using 532 nm excitation wavelength. The scattered light was dispersed in a 0.5 m imaging spectrograph (Acton, SpectraPro 2555i). The signal was detected with an EMCCD camera (Andor Newton EM DU971N−BV) using a 60 μm slit width. The signal was accumulated from 200 measurements 2 s each to obtain a good signal-to-noise ratio.

Transport Measurements. The transport measurements were done in a home-built liquid helium measurement system, which allows covering the whole temperature range from room temperature down to 4.2 K. We used two-terminal measurements, applying a drain-source voltage while measuring the current response through the CNTs with a current preamplifier. A small drain-source voltage of 10 mV was used for all samples when measuring the gate response of each nanotube.

Results

Data from four individual CNTs are presented. Two of them are metallic (M1 and M2), and two of them are semiconducting (S1 and S2). Raman spectra and the results of electronic transport measurements are presented below.

Sample M1. The Raman spectrum from sample M1, shown in Figure 2a, is measured using a 632.8 nm (1.96 eV) excitation. No signals were seen when using a 532.0 nm (2.33 eV) excitation. The structure of the G mode suggests that the tube is metallic as evidenced by the broad double peak structure with maxima at 1537.9 and 1589.2 cm^{-1}. The RBM is very sharp, and it lies at 220 cm^{-1}. The diameter d calculated from RBM position by using eq 1 is 1.08 nm[25]

$$d = \frac{217.8\ \mathrm{cm}^{-1}}{\omega_{RBM} - 15.7\ \mathrm{cm}^{-1}} \quad (1)$$

where ω_{RBM} is the measured RBM frequency. The AFM measurement yielded the diameter of 0.8 ± 0.2 nm, which agrees reasonably well with the Raman measurement. The D mode at 1321.6 cm^{-1} is relatively strong indicating the presence of defects in the tube. The assignment of chiral indices was made by comparing the measured RBM frequency and the used excitation energy E_l to RBM frequencies and transition energies E_{ii} determined by Maultzsch et al.[26,27] In determining the possible resonant tubes it was assumed that the SWNT should have E_{ii} within a resonant window E_l ± 0.10 eV.[25,26,28] According to this analysis, there are two possible candidates with chiral indices of (13,1) or (12,3). From these we choose as a likely candidate the (13,1) tube on the basis of the close match of the RBM frequencies (220 cm^{-1} in this work, 221 cm^{-1} in ref 26). The E_{11} transition energy for this tube was calculated to be 2.06 eV.[26]

In the transport measurements, shown in Figure 2b, sample M1 displays very weak gate dependence throughout the range −10 to 10 V. Combined with a linear $I-V$ at room temperature (shown in the inset), which translates into a device resistance of close to 125 kΩ, the transport data confirms the view of M1 being metallic. As the sample is cooled down the gate dependence stays weak, while the resistance increases gradually. At 140 and 75 K, the current response display clear oscillations along the full gate scan range. Performing a fast Fourier transform (FFT) on the data gives one well-defined peak with a period of 241 mV. At 4.2 K, the device resistance has increased to around 10 MΩ or more, and the oscillations are no longer clearly visible. An FFT on the data, however, reveals that the period of 241 mV still gives the strongest peak, but also other peaks are emerging. Turning the attention back to the $I-V$ characteristics displayed in the inset of Figure 2b, it is noted that a nonlinear behavior develops at low temperatures. At 4.2 K, a plateau in the current response is present, centered

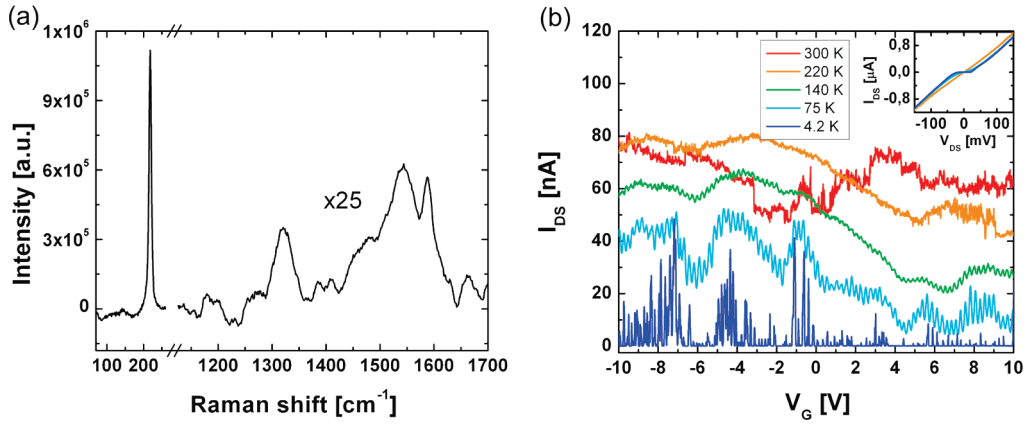

Figure 2. (a) Raman spectrum from sample M1. The right-hand section of the curve has been smoothed and multiplied by a factor of 25 for clarity. (b) Corresponding drain-source current versus back gate voltage at constant source drain bias voltage of 10 mV. The color of each trace shows the sampling temperature. Inset: $I-V$ characteristics at two different temperatures.

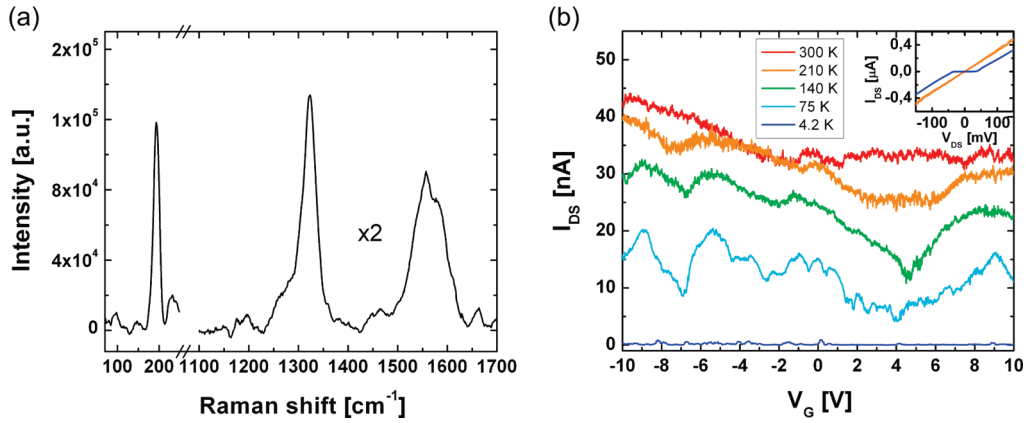

Figure 3. (a) Raman spectrum from sample M2. The right-hand section of the curve has been multiplied by a factor of 2 for clarity. (b) Corresponding drain-source current versus back gate voltage at constant source drain bias voltage of 10 mV. The color of each trace shows the sampling temperature. Inset: $I-V$ characteristics at three different temperatures.

at zero source-drain voltage with a width of about 40 mV. The increasing sample resistance with decreasing temperature, the oscillations in transconductance and nonlinear $I-V$ characteristics at low temperatures are likely due to Coulomb blockade caused by a quantum dot formation along the SWNT.[29] Usually several such dots are formed between the electrodes due to defects along the SWNT and the formation of tunneling barriers at the contacts between the nanotube and the electrodes. In this case, though, apparently one dot is dominating.

Sample M2. The Raman spectrum from sample M2 shown in Figure 3a is measured using a 632.8 nm (1.96 eV) excitation. No signals were seen when using a 532.0 nm (2.33 eV) excitation. The shape of the G mode clearly suggests that the tube is metallic and the RBM at 193.9 cm^{-1} gives a diameter of 1.22 nm. while the AFM measurement yielded a diameter of 1.0 ± 0.2 nm. The large intensity of the D mode at 1322.0 cm^{-1} indicates a substantial amount of defects in the tube. The index assignment was made as for the previous sample and this tube is assigned to the chiral indices of (13,4) with a E_{11} transition energy of 1.944 eV.

The electronic transport measurements on M2 are shown in Figure 3b. This tube has also weak response to gate voltage and a linear $I-V$ characteristics at room temperature (see inset), indicating that the tube is metallic. As the temperature is lowered, the overall resistance of the sample increases from 298 kΩ at room temperature to above 10 MΩ at 4.2 K. However, this tube does not show any regular oscillations as a function of gate voltage, and an FFT does not reveal any periodic behavior in its fluctuations, probably due to a less clear formation of a dominating quantum dot than in the case of M1. From the isotherms of the $I-V$ characteristics (see inset of Figure 3b), this tube exhibits nonlinear dependence at low temperatures. At 4.2 K, a plateau has formed in the low bias regime with a width of ∼60 mV. This may be explained by the SWNT not being fully metallic in nature. Theoretical predictions based on tight-binding calculations for the p_π orbitals alone have classified all SWNTs with chiral indices fulfilling the condition $m - n = 3 \times$ integer as semimetallic with zero band gap.[30,31] In fact, a more detailed consideration has shown that only armchair SWNTs are truly metallic, while remaining "metallic" SWNTs may possess curvature induced band gaps on the order of tens of millivolts.[32−34] This nanotube, with the ascribed indices (13,4), falls into this category. On the basis of the low-temperature $I-V$ characteristics, we estimate that the band gap is close to 30 meV. This value is in excellent agreement with the theoretically predicted value of 31 meV.[34]

Sample S1. The Raman spectrum of this tube is shown in Figure 4a, and it is measured using 532 nm (2.33 eV) excitation wavelength. No signals were seen when using 632.8 nm (1.96 eV) excitation. The G mode of the Raman spectrum suggests that the tube is semiconducting. The most notable feature in the G mode is that the G^- band at 1559.8 cm^{-1} is more intense than the G^+ band at 1587.3 cm^{-1}. Usually the G^+ band is stronger. The RBM peak at 103.5 cm^{-1} gives a diameter of 2.48 nm, while the AFM measurement gives the diameter of 2.7 ± 0.2 nm. The D band at 1345 cm^{-1} is rather weak indicating a relatively defect-free tube.

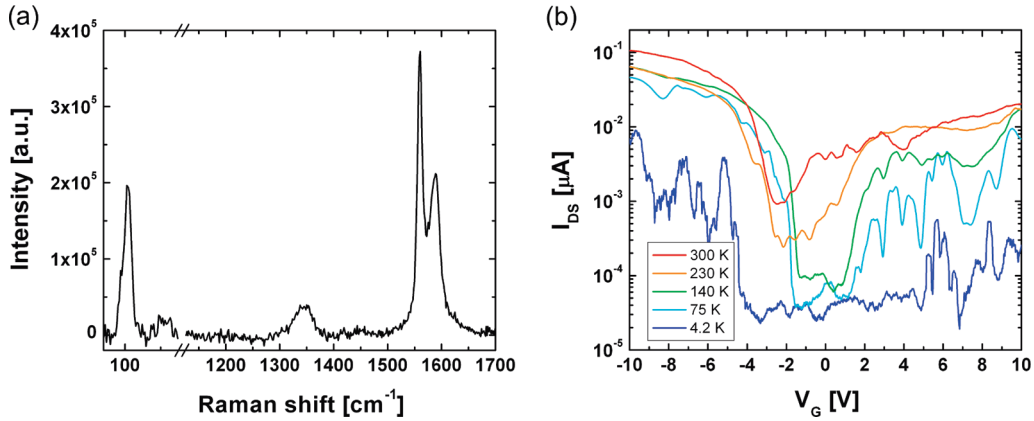

Figure 4. (a) Raman spectrum from sample S1. (b) Corresponding drain-source current versus back gate voltage at constant source drain bias voltage of 10 mV. The color of each trace shows the sampling temperature.

The index assignment was attempted by comparing the excitation energy with the energies of E_{55} and E_{66} transitions. These energies were calculated by using an equation obtained for low-E_{ii} transitions[25,35]

$$E_{ii}(p, d_t) - \frac{\beta_p \cos(3\theta)}{d_t^2} = a\frac{p}{d_t}\left[1 + b \log \frac{c}{p/d_t}\right] \quad (2)$$

where θ is the chiral angle, d_t is the diameter, $a = 1.049$ eV·nm, $b = 0.456$, and $c = 0.812$ nm^{-1}. For higher transitions, a correction term given by $\Delta E = \gamma/d_t$ with $\gamma = (0.305 \pm 0.004$ eV) has been found necessary to reproduce experimental data.[25] We used this correction together with eq 2 (using $p = 7, 8$) in order to estimate the transition energies for E_{55} and E_{66}. The value of parameter β_p was obtained by extrapolating the data of Figure 1e of ref 25 to $p = 7,8$. As expected for higher transitions and thicker tubes it is not possible to assign the chiral indices definitely but potential candidates include (21,19), (24,16), and (22,17).

The transport measurements for sample S1 are shown in Figure 4b. With a constant drain-source voltage of 10 mV, the drain-source current traces show a clear gap feature in response to sweeping the gate voltage. Within the gap feature, the current response is suppressed with decreasing temperature. At most, the drain-source current is modulated more than 3 orders of magnitude. Thus, this sample is confirmed to have semiconducting properties, as predicted in the Raman measurement.

Sample S2. The Raman spectrum shown in Figure 5a is measured using 532 nm (2.33 eV) excitation wavelength. The shape of the G band indicates clearly that the tube is semiconducting and the D band is relatively weak. The RBM peak at 133.1 cm^{-1} gives the diameter of 1.9 nm while the AFM measurement suggests that the diameter would be 2.6 ± 0.2 nm in significant disagreement with the Raman measurement. For this tube, Raman spectrum was also observed when using 632.8 nm (1.96 eV) excitation wavelength as shown in Figure 5b. Interestingly, the G band region obtained with 632.8 nm excitation is totally different from the spectrum obtained with 532 nm excitation but for both excitation wavelengths the RBM mode has the same frequency within the calibration accuracy. When using 632.8 nm excitation, another very weak band is also observed in the RBM region at 97.0 cm^{-1} as shown in Figure 5c. This corresponds to a diameter of 2.68 nm according to eq 1. This is in a good agreement with the AFM measurement and gives strong evidence that S2 tube is actually a bundle of two tubes or a double-walled nanotube. For 632.8 nm excitation, the G band region shows a similar anomalous intensity ratio for the G^- and G^+ bands as for the S1 tube. Since the spectrum is totally different from the one obtained with 532 nm excitation it is most probably dominated by the larger tube. The index assignment will be discussed in detail in the Discussion section.

The corresponding electronic transport measurements are shown in Figure 5d. Here the source-drain current response is plotted on a log scale versus applied gate voltage, for a constant drain-source voltage of 10 mV. A clear and strong gate dependency is seen for this tube, spanning more than 2 orders of magnitude at intermediate temperatures, which confirms the prediction from Raman measurements that the tube is semiconducting. The data show an ambipolar signature with a somewhat stronger p-type behavior and a gap feature visible already at room temperature. At the lowest temperature of 4.2 K, the overall resistance is suppressed also for this sample.

In total, two SWNTs showed metallic and two of them showed semiconducting behavior. The properties of the devices are summarized in Table 1.

Discussion

In this study we successfully combined two independent methods, Raman spectroscopy and electronic transport measurements, to study the basic properties of isolated SWNTs. A similar approach has previously been used to investigate the electron−phonon coupling and the correlation between the Raman and transport measurements for metallic and semiconducting tubes.[36] Raman spectroscopy has also been used to identify the tube type of an individual contacted nanotube in connection with photoconductivity studies.[37] Electrochemical gating of individual SWNTs was observed by electron transport and Raman measurements, but not from the same individual tubes.[38] Recently, there has been much interest in the dependence of the G-band and G′-band on the applied gate potential in individual SWNTs.[17−19,23] This kind of studies give detailed information on Fermi level shifting and electron−phonon coupling in isolated SWNTs. However, in none of these studies were low-temperature transport measurements applied in connection with Raman measurements of individual SWNTs. This kind of combination can be used to test not only the correlation between the Raman measurements and transport measurements on the metallic/semiconducting behavior of the tubes but also to obtain information on the small band gap present in nonarmchair ($n \neq m$) metallic SWNTs.[33] In addition, it is still important to make further tests on the metallic/semimetallic

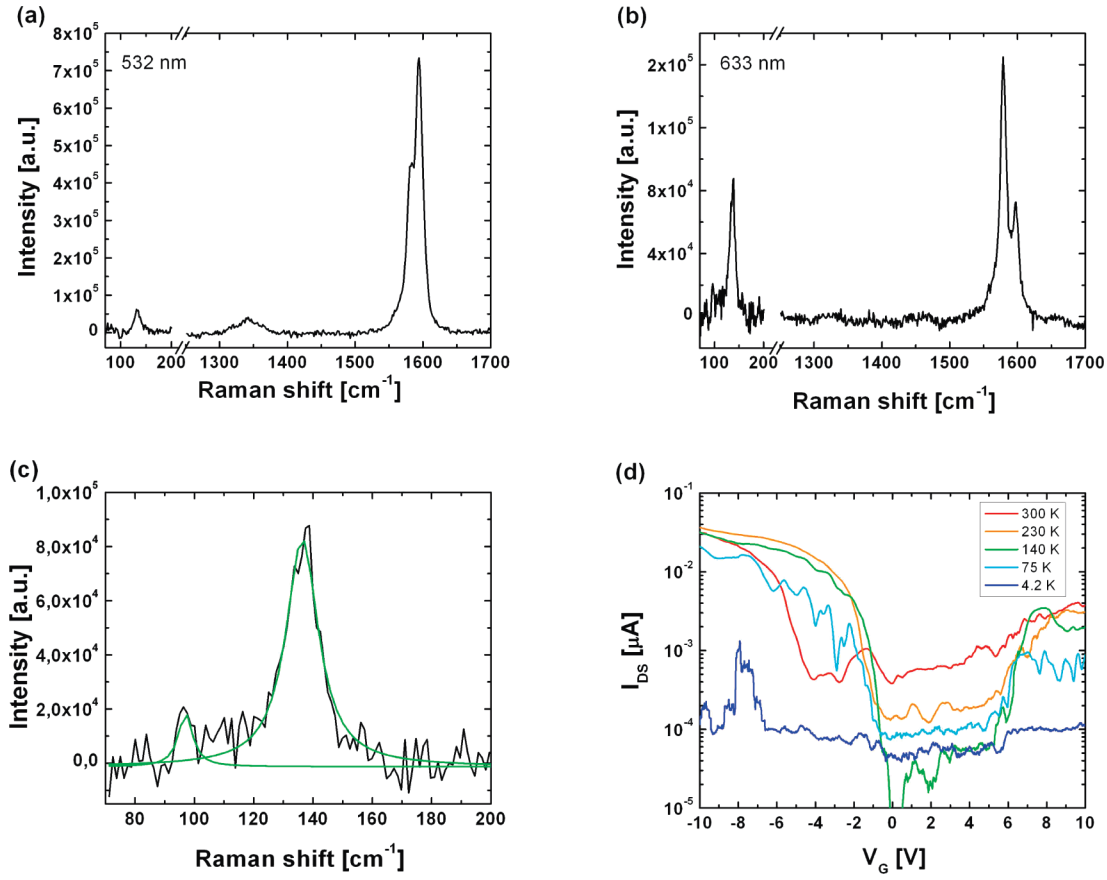

Figure 5. (a) Raman spectrum from sample S2 measured by using 532 nm excitation, (b) Raman spectrum of the same sample by using 632.8 nm excitation, (c) Raman spectrum of the RBM region observed by using 632.8 nm excitation. Green lines show Lorentzian fits to the data; (d) Corresponding drain-source current versus back gate voltage at constant source drain bias voltage of 10 mV. The color of each trace shows the sampling temperature.

TABLE 1: Data Collected from Raman Spectra, Electronic Transport, and AFM Measurement on Four Different Carbon Nanotubes

sample	M1	M2	S1	S2
(n, m)	(13,1) or (12,3)	(13,4)	[a]	[a]
RBM (cm^{-1})	218.3	193.9	103.5	133.1 97.0
d_{RBM} (nm)[b]	1.08	1.22	2.48	1.85 2.68
d_{RBM} (nm)[c]	1.07	1.22	2.67	1.92 2.91
d_{AFM} (nm)	0.8	1.0	2.7	1.8 2.6
length (nm)	360	750	880	850
D mode (cm^{-1})	1321.6	1322.0	1345.5	1341.1
G mode (cm^{-1})	1537.9/ 1589.2	1554.1/ 1587.7	1559.8/ 1587.3	1578.9/ 1592.2 (532 nm) 1579.1/ 1597.7 (633 nm)
resistance (kΩ)[d]	125	298	478	52.6 × 10^3

[a] Several possibilities of (n, m) assignment. [b] Calculated from RBM using eq 1. [c] Calculated from RBM using eq 3. [d] Room temperature value in the zero drain-source voltage limit.

behavior of the same individual tubes with two independent methods since, as pointed out by Wu et al., metallic tubes do not necessarily always have a broadened G-band and thus one-to-one correspondence between line broadening and metallic character is invalid.[39]

In our samples made by spin-depositing substrates with very dilute nanotube solution, individual isolated tubes set on the substrates.[40] With the used laser excitation spot having a diameter of ~500 nm, it is easy to separate the Raman signals coming from different tubes. The polarization of the excitation light also helps to discriminate the signals between tubes since for the parallel (with tube axis) polarization the signal is greatly enhanced compared to the perpendicular geometry.[12,24,41−46] In this study the contacted tubes were well separated from other tubes except in one case (S1) where another tube was in the close vicinity of the measured tube, as shown in Figure 1. In this case, the signals from the two tubes were easily separable by scanning the excitation spot back and forth over the tubes in which case two separate signals and their combination could be seen depending on the position of the laser beam with respect to the tubes. In addition, the polarization of the excitation beam was selected to be parallel with the desired tube axis which suppressed the signal significantly from the other tube which was almost in perpendicular position compared to S1.

It is notable that in our study both the Raman and the transport measurements are in perfect agreement when determining the metallic/semiconducting character of the tubes. Thus, out of four studied tubes, two were metallic and two were semiconducting, as determined by both methods. The diameters of the tubes calculated from RBM frequencies also correspond well with the diameters measured with AFM in all cases. In the case of S2 the observation of two distinct RBM frequencies corresponding to diameters of 1.9 and 2.7 nm suggests that it is a bundle of two tubes or a double-walled nanotube. The AFM measurement gives a diameter of 2.6 nm which is in excellent agreement with the diameter of the larger tube from RBM measurement. The interplanar spacing in natural graphite is 3.35 Å according to which a tube with 1.9 nm diameter would fit well inside a tube with 2.7 nm diameter.[47] On the other hand, in the AFM measurement, there is a clear shoulder in the

cross-section of the tube corresponding to a diameter of 1.8 nm. This shoulder was observed in several locations along the nanotube. This corresponds well with the diameter of the smaller tube determined from the frequency of the RBM mode. A similar shoulder was not observed for other tubes when measured with the same tip. Thus, it seems plausible that S2 is a bundle of two SWNTs.

For the metallic tubes, the most interesting information of the transport measurements is related to the behavior at low temperatures since the signature of a possible small band gap is expected to appear there.[33,48] For the M1 tube the predicted small band gap is 50 (13,1 tube) or 43 meV (12,3 tube), depending on the assignment.[34] Thus, the signature of the band gap should be visible in the low-temperature transport measurements. However, in this case, the strong signal due to the Coulomb blockade phenomenon masks possible signals originating from the small band gap. On the other hand, for M2, the oscillations due to Coulomb blockade are absent and the band gap was estimated to be 30 meV, being in excellent agreement with the theoretical prediction for the band gap (31 meV).[34] From sample M1 we can estimate the gate efficiency factor, $\alpha = V_{max}/\Delta V_{gate}$, where V_{max} is the maximum drain-source voltage for which resonant tunneling occurs and ΔV_{gate} is the gate voltage difference between consecutive resonant tunneling peaks.[32] As a lower bound of V_{max} we have 20 mV from the low temperature $I-V$ curve and ΔV_{gate} is 241 mV. We then get that $\alpha \geq 20/241 = 0.083$. All four samples have the same substrate and therefore the same gate efficiency factor. We can now for samples M2, S1, and S2 take the theoretical band gap values determined from the ascribed (n, m) indices, see Table 1, and calculate the upper bound of ΔV_{gate} for traversing the band gap. We get $\Delta V_{gate} \leq 0.37$, 5.90, and 7.47 V, respectively. Inspection of the gate dependent transport data shows that the gap features all fall within these limits. Thus, the argued interpretation of the data seems consistent.

The sample S1 possesses several interesting features. First of all, it is a very thick tube. The estimate from the measured RBM position gives 2.5 nm, and the AFM measurement indicates the thickness of 2.7 nm. The RBM mode at 103.5 cm^{-1} is surprisingly intense keeping in mind that, generally, the RBM mode for thick tubes is very difficult to observe.[24] In previous Raman studies of individual SWNTs the RBM frequency varied between 332 and 95 cm^{-1} corresponding to diameters between 0.7 and 3.0 nm.[25,24,28,50−53] As far as we know, there is only one report of an observation of a lower frequency of the RBM mode than in the present case, namely 95 cm^{-1} assigned unambiguously to the (23, 21) tube by electron diffraction.[53] The second interesting feature of the S1 tube is that it shows an unusual intensity ratio for ω_G^- and ω_G^+ bands. Normally, for semiconducting tubes the ratio $I\omega_{G-}/I\omega_{G+}$ is between 0.1 and 0.3,[24] but in our case it is 1.6. Jorio et al. reported similar effect for a few tubes with diameter of 1.60 ± 0.05 nm when using excitation of 514.5 nm (2.41 eV).[24] They explained the phenomenon with a special resonance condition where the electronic transition energy E_{ii}^S satisfies the resonance condition for the incident photon and the lower energy electronic transition $E_{(i-1)(i-1)}^S$ satisfies the resonance condition for the scattered photon. If one of the G-band modes is very close to the scattered photon energy, this particular mode will be strongly enhanced. According to this mechanism, the E_{ii}^S and $E_{(i-1)(i-1)}^S$ transitions should lie within the phonon energy for the specific tube in question. Judging from the Kataura plot the specific resonance condition is indeed fulfilled for the E_{44}^S and E_{33}^S for the tubes with a diameter of 1.60 nm. Interestingly, on the basis of the Kataura plot, Jorio et al. predicted that this phenomenon should be observable for tubes with a diameter close to 2.5 nm with the excitation energy of 2.54 eV. In our case the S1 tube diameter ($d_t = 2.48$ nm according to RBM) is indeed very close to this and the used excitation energy (2.33 eV) is in a correct range. In this case the special resonance occurs between E_{66}^S and E_{55}^S transitions.[8] Thus, our observation strongly corroborates the explanation presented by Jorio et al. and generalizes the idea. However, if we inspect the Kataura plot from ref 24 or calculate the transition energies by using eq 1 for the tube diameter of 2.5 nm, the transition energy E_{66}^S is actually a little bit too high to fit the observations. Instead, for a diameter of 2.65−2.7 nm the calculated transitions fit very well. Note that the AFM measurement gives the diameter of 2.7 nm for this tube. In this case the possible chiralities include (21,19), (24,16), or (22,17), but the absolute assignment cannot be done with certainty. Nevertheless, there are several tubes that can fulfill the special resonance condition. The slight discrepancy in the diameter suggests that either the equation to calculate RBM or the Kataura plot needs some refinement. In fact, in the measurements of RBM modes from the tubes with precisely known structure determined by electron diffraction, it was found that the generally used relations between the diameter and RBM frequency tend to underestimate the tube diameter for thick tubes.[53] Using the data from ref 53 gives a diameter of ∼2.7 nm for the S1 tube, which is in perfect agreement with the interpretation of anomalous intensity of the G-band components and also with the AFM measurement. Thus, our findings suggest that the used RBM relations should be refined for large diameter tubes. Our results are in good agreement with the relation given in ref 53

$$d = \frac{204\ \text{cm}^{-1}}{\omega_{RBM} - 27\ \text{cm}^{-1}} \quad (3)$$

which was derived using suspended tubes.

As mentioned above, the S2 tube is most probably a bundle of two SWNTs, based on the observation of two RBM modes and two corresponding diameters in the AFM measurement. First we consider the observation of the RBM mode at 133.1 cm^{-1} with both 532 and 632.8 nm excitation. This requires that the tube in question has a resonant transition for both excitation energies. Inspection of a Kataura plot shows that the relevant transitions must be E_{33} and E_{44}. By using eq 2, several possible candidates are found, including (16,11) and (14,13), but again a definite assignment is not possible. The observation of anomalous G-band shape for the 632.8 nm excitation can only be explained if the spectrum is a superposition of the smaller and larger tubes and the larger tube dominates the appearance of the spectrum since it is impossible to satisfy simultaneously that the smaller tube is resonant with both excitation wavelengths and that it also would have a special resonance condition which gives rise to the anomalous intensity ratio for the G-band components. For the larger tube, the special resonance condition can be expected just as for the S1 tube which has a similar diameter. However, since the special resonance condition is observed for the 632.8 nm excitation the tube thickness must be larger than for the S1 tube as indeed is the case based on the RBM frequencies. Using eq 3 a thickness of 2.91 nm is obtained for S2. Then, by using eq 2 again several candidates are found that could satisfy the special resonance condition including the previously mentioned (21,19), (24,16), and (22,17). Thus, with this interpretation all the observations are compatible with each other.

Conclusions

Three individual SWNTs and one bundle of two nanotubes were investigated by Raman spectroscopy and temperature-dependent electric transport measurements. Two of the tubes

were metallic, and two of them were semiconducting, as determined by both methods independently. The diameter of the tubes varied between 1.1 and 2.9 nm. The low-temperature transport measurements revealed a coulomb blockade phenomenon for one of the metallic tubes and provided some evidence of a small band gap (~30 meV) for the other metallic tube, assigned to the chiral indices (13,4) by Raman measurements, in accordance with theoretical predictions of the existence of a small band gap of 31 meV for this tube. For the semiconducting tubes having a diameter of 2.7−2.9 nm, a special resonance condition was observed which causes an anomalous intensity ratio for the two components of the G-band, an effect observed previously by Jorio et al. for a few tubes with a diameter of 1.6 nm.[24] Our findings support the explanation of the effect given in ref 24 and suggest that the effect is common for thick tubes. Analysis of the data for thick tubes provides evidence that the currently used relations between the frequency of the radial breathing mode and the tube diameter tend to underestimate the diameter for thick tubes. On the basis of our findings the preferred expression for thicker tubes is $\omega_{RBM} = 204/d + 27$ derived by Meyer et al.[53]

Acknowledgment. This work was funded by the Academy of Finland via the FinNano program and the research consortium Molecular Electronics and Photonics (MEP, Decisions No. 118232 and 117937).

References and Notes

(1) Reich, S.; Thomsen, C.; Maultzsch, J. *Carbon Nanotubes: Basic Concepts and Physical Properties*; Wiley-VCH: Weinheim, 2004.
(2) Dresselhaus, M. S.; Eklund, P. C. *Adv. Phys.* **2000**, *49*, 705.
(3) Jorio, A.; Pimenta, M. A.; Souza Filho, A. G.; Saito, R.; Dresselhaus, G.; Dresselhaus, M. S. *New J. Phys.* **2003**, *5*, 139.
(4) Rao, A. M.; Richter, E.; Bandow, S.; Chase, B.; Eklund, P. C.; Williams, K. W.; Fang, S.; Subbaswamy, K. R.; Menon, M.; Thess, A.; Smalley, R. E.; Dresselhaus, G.; Dresselhaus, M. S. *Science* **1997**, *275*, 187.
(5) Dresselhaus, M. S.; Dresselhaus, G.; Jorio, A. *J. Phys. Chem. C* **2007**, *111*, 17893.
(6) Kneipp, K.; Kneipp, H.; Corio, P.; Brown, S. D. M.; Shafer, K.; Motz, J.; Perelman, L. T.; Hanlon, E. B.; Marucci, A.; Dresselhaus, G.; Dresselhaus, M. S. *Phys. Rev. Lett.* **2000**, *84*, 3470.
(7) Jorio, A.; Saito, R.; Hafner, J. H.; Lieber, C. M.; Hunter, M.; McClure, T.; Dresselhaus, G.; Dresselhaus, M. S. *Phys. Rev. Lett.* **2001**, *86*, 1118.
(8) Kataura, H.; Kumazawa, Y.; Maniwa, Y.; Umezu, I.; Suzuki, S.; Ohtsuka, Y.; Achiba, Y. *Synth. Met.* **1999**, *103*, 2555.
(9) Kataura, H.; Kumazawa, Y.; Kojima, N.; Maniwa, Y.; Umezu, I.; Masubuchi, S.; Kazama, S.; Zhao, X.; Ando, Y.; Ohtsuka, Y.; Suzuki, S.; Achiba, Y. Optical absorption and resonant Raman scattering of carbon nanotubes. In *Electronic Properties of Novel Materials-Science and Technology of Molecular Nanostructures, Proceedings of the XIII International Winter School on Electronic Properties of Novel Materials (IWEPNM'99)*; Kuzmany, H., Mehring, M., Fink, J., Roth, S., Eds.; American Institute of Physics: Woodbury, NY, 1999; p 328.
(10) Samsonidze, G. G.; Saito, R.; Kobayashi, N.; Grüneis, A.; Jiang, J.; Jorio, A.; Chou, S. G.; Dresselhaus, G.; Dresselhaus, M. S. *Appl. Phys. Lett.* **2004**, *85*, 5703.
(11) Popov, V. N.; Henrard, L.; Lambin, P. *Nano Lett.* **2004**, *4*, 1795.
(12) Saito, R.; Dresselhaus, G.; Dresselhaus, M. S. *Physical Properties of Carbon Nanotubes*; Imperial College Press: London, 1998.
(13) Liang, W.; Bockrath, M.; Bozovic, D.; Hafner, J. H.; Tinkham, M.; Park, H. *Nature* **2001**, *411*, 665.
(14) Das, A.; Sood, A. K.; Govindaraj, A.; Saitta, A. M.; Lazzeri, M.; Mauri, F.; Rao, C. N. R. *Phys. Rev. Lett.* **2007**, *99*, 136803.
(15) Liang, C.-W.; Lee, W.-Y.; Tsai, C.-H.; Roth, S. *Phys. Status Solidi B* **2008**, *245*, 2209.
(16) Ding, L.; Tselev, A.; Wang, J.; Yuan, D.; Chu, H.; McNicholas, T. P.; Li, Y.; Liu, J. *Nano Lett.* **2009**, *9*, 800.
(17) Bushmaker, A. W.; Deshpande, V. V.; Bockrath, M. W.; Cronin, S. B. *Nano Lett.* **2007**, *7*, 3618.
(18) Tsang, J. C.; Freitag, M.; Perebeinos, V.; Liu, J.; Avouris, P. H. *Nat. Nanotechnol.* **2007**, *2*, 725.
(19) Khoi, T.; Nguyen, A. G.; Moonsub, S. *Phys. Rev. Lett.* **2007**, *98*, 145504.
(20) Ward, D. R.; Halas, N. J.; Ciszek, J. W.; Tour, J. M.; Wu, Y.; Nordlander, P.; Natelson, D. *Nano Lett.* **2008**, *8*, 919.
(21) Yuan, S.; Zhang, Q.; You, Y.; Shen, Z.-X.; Shimamoto, D.; Endo, M. *Nano Lett.* **2009**, *9*, 383.
(22) Bushmaker, A. W.; Deshpande, V. V.; Hsieh, S.; Bockrath, M. W.; Cronin, S. B. *Nano Lett.* **2009**, *9*, 607.
(23) Kalbac, M.; Kavan, L.; Farhat, H.; Kong, J.; Dresselhaus, M. S. *J. Phys. Chem. C* **2009**, *113*, 1751.
(24) Jorio, A.; Souza Filho, A. G.; Dresselhaus, G.; Dresselhaus, M. S.; Swan, A. K.; Ünlü, M. S.; Goldberg, B. B.; Pimenta, M. A.; Hafner, J. H.; Lieber, C. M.; Saito, R. *Phys. Rev. B* **2002**, *65*, 155412.
(25) Araujo, P. T.; Doorn, S. K.; Kilina, S.; Tretiak, S.; Einarsson, E.; Maruyama, S.; Chacham, H.; Pimenta, M. A.; Jorio, A. *Phys. Rev. Lett.* **2007**, *98*, 067401.
(26) Maultzsch, J.; Reisch, S.; Hennrich, F.; Thomsen, C. *Phys. Rev. B* **2005**, *72*, 205438.
(27) Supporting Information of ref 26 (EPAPS Document No. E-PRBMDO-72-109544). This document can be reached via a direct link in the online article's HTML reference section or via the EPAPS home page http://www.aip.org/pubservs/epaps.html.
(28) Jorio, A.; Saito, R.; Hafner, J. H.; Lieber, C. M.; Hunter, M.; McClure, T.; Dresselhaus, G.; Dresselhaus, M. S. *Phys. Rev. Lett.* **2001**, *86*, 1118.
(29) Bockrath, M.; Cobden, D. H.; McEuen, P. L.; Chopra, N. G.; Zettl, A.; Thess, A.; Smalley, R E. *Science* **1997**, *275*, 1922.
(30) Saito, R.; Fujita, M.; Dresselhaus, G.; Dresselhaus, M. S. *Appl. Phys. Lett.* **1992**, *60*, 2204.
(31) Hamada, N.; Sawada, S.; Oshiyama, A. *Phys. Rev. Lett.* **1992**, *68*, 1579.
(32) Kane, C. L.; Mele, E. J. *Phys. Rev. Lett.* **1997**, *78*, 1932.
(33) Zhou, C.; Kong, J.; Dai, H. *Phys. Rev. Lett.* **2000**, *84*, 5604.
(34) Sasaki, K.; Saito, R.; Dresselhaus, G.; Dresselhaus, M. S.; Farhat, H.; Kong, J. *Phys. Rev. B* **2008**, *78*, 235405.
(35) Kane, C. L.; Mele, E. J. *Phys. Rev. Lett.* **2004**, *93*, 197402.
(36) Oron-Carl, M.; Hennrich, F.; Kappes, M. M.; Löhneysen, H. v.; Krupke, R. *Nano Lett* **2005**, *5*, 1761.
(37) Balasubramanian, K.; Fan, Y.; Burghard, M.; Kern, K.; Friedrich, M.; Wannek, U.; Mews, A. *Appl. Phys. Lett.* **2004**, *84*, 2400.
(38) Cronin, S. B.; Barnett, R.; Tinkham, M.; Chou, S. G.; Rabin, O.; Dresselhaus, M. S.; Swan, A. K.; Ünlü, M. S.; Goldberg, B. B. *Appl. Phys. Lett.* **2004**, *84*, 2052.
(39) Wu, Y.; Maultzsch, J.; Knoesel, E.; Chandra, B.; Huang, M.; Sfeir, M. Y.; Brus, L. E.; Hone, J.; Heinz, T. F. *Phys. Rev. Lett.* **2007**, *99*, 027402.
(40) Giordani, S.; Bergin, S. D.; Nicolosi, V.; Lebedkin, S.; Kappes, M. M.; Blau, W. J.; Coleman, J. N. *J. Phys. Chem. B* **2006**, *110*, 15708.
(41) Gommans, H.; Alldredge, J. W.; Tashiro, H.; Park, J.; Magnuson, J.; Rinzler, A. G. *J. Appl. Phys.* **2000**, *88*, 2509.
(42) Ajiki, H.; Ando, T. *Physica B* **1994**, *201*, 349.
(43) Duesberg, G. S.; Loa, I.; Burghard, M.; Syassen, K.; Roth, S. *Phys. Rev. Lett.* **2000**, *85*, 5436.
(44) Hwang, J.; Gommans, H. H.; Ugawa, A.; Tashiro, H.; Haggenmueller, R.; Winey, K. I.; Fischer, J. E.; Tanner, D. B.; Rinzler, A. G. *Phys. Rev. B* **2000**, *62*, R13−310.
(45) Yu, Z.; Brus, L. E. *J. Phys. Chem. B* **2001**, *105*, 1123.
(46) Jorio, A.; Souza Filho, A. G.; Brar, V. W.; Swann, A. K.; Ünlü, M. S.; Goldberg, B. B.; Righi, A.; Hafner, J. H.; Lieber, C. M.; Saito, R.; Dresselhaus, G.; Dresselhaus, M. S. *Phys. Rev. B* **2002**, *65*, 121402.
(47) Girifalco, L. A.; Lad, R. A. *J. Chem. Phys.* **1956**, *25*, 693.
(48) Cao, J.; Wang, Q.; Dai, H. *Nat. Mater.* **2005**, *4*, 745.
(49) Telg, H; Maultzsch, J.; Reich, S.; Hennrich, F.; Thomsen, C. *Phys. Rev. Lett.* **2004**, *93*, 189901.
(50) Haroz, E. H.; Bachilo, S. M.; Weisman, R. B.; Doorn, S. K. *Phys. Rev. B* **2008**, *77*, 125405.
(51) Hennrich, F.; Krupke, R.; Lebedkin, S.; Arnold, K.; Fischer, R.; Resasco, D. E.; Kappes, M. M. *J. Phys. Chem. B* **2005**, *109*, 10567.
(52) Paillet, M.; Michel, T.; Meyer, J. C.; Popov, V. N.; Henrard, L.; Roth, S.; Sauvajol, J.-L. *Phys. Rev. Lett.* **2006**, *96*, 257401.
(53) Meyer, J. C.; Paillet, M.; Michel, T.; Moréac, A.; Neumann, A.; Duesberg, G. S.; Roth, S.; Sauvajol, J.-L. *Phys. Rev. Lett.* **2005**, *95*, 217401.

JP9034985